

Research Article

Studying Behavior of Exterior RC Beam–Column Joints Strengthened Using CFRP for Achieving “Strong Column-Weak Beam” In RC Frames

Mohammed A. Sakr¹, Ayman A. Selemah¹, Tarek M. Khalifa², Galal EL-Samak³

¹Prof. Department of Structural Engineering, Tanta University, Tanta, Egypt.

²Lecturer, Department of Structural Engineering, Tanta University, Tanta, Egypt.

³Assistant Lecturer, Department of Civil Engineering, Kafrelsheikh University, Kafrelsheikh, Egypt.

*Corresponding Author

Mohammed A. Sakr

Abstract: This paper presents an experimental and numerical study for the cyclic structural performance of RC exterior beam–column joints strengthened using CFRP sheets taken into account the two possible debonding failure modes, either by sheet end debonding or concrete cover separation in addition to the traditional failure modes such as shear failure, flexural failure or joint shear failure. The present experimental program consists of testing eight 2/3 scale specimens; namely, a control specimen which is designed using weak column-strong beam philosophy, and seven strengthened specimens which are showed various types of failures. Also a nonlinear 2D-finite element (FE) analysis which is able to predict the debonding failure modes was established, a good agreement is observed between the FE results and experimental observations. Experimental and numerical results indicate that strengthening using CFRP sheets increases the maximum load but, in some cases, may change the failure pattern of RC connections to an unacceptable mode of failure which must be avoided.

Keywords: Beam–Column Joint, CFRP, Reinforced Concrete, Strengthening, Cyclic Behavior, Nonlinear FE Analysis.

INTRODUCTION

The seismic lateral loading substantial forces are focused in the small-sized structural members of the beam-to-column joints of RC buildings. Moreover, inappropriate, crosswise reinforcement in the joint is the main reason for the detected joint shear failures during latest earthquakes, The Cairo earthquake, Egypt in 1992 is a good example for such type of failures. In addition, because of the lack of capacity design approach, the adjacent beams were usually stronger than the columns of older structures. Thus, after strengthening joints of these frames the seismic damages were in most of such cases are localized in the lower part of the columns or just above the floor slab rather than the beam. Joint shear or column hinging failures are considered as unacceptable failure mechanisms of reinforced concrete moment-resisting frames. So the problem about strengthening of beam-column connections by increasing the capacity of those zones by CFRP, with the objective of relocating the potential plastic hinges to the beams without occurrence of debonding or rupture for CFRP sheets needs to be investigated in depth. Debonding of CFRP sheets either by concrete cover

separation (separation at the surface between the reinforcing steel and the concrete cover) or by sheet debonding from concrete substrate is an important issue in CFRP-strengthened concrete structures.

FRP composites are used extensively for strengthening RC structures worldwide. This popular agreement is mostly because of the inherent advantage of FRP such as greater reinforcement, light weight, simplicity of application and high erosion resistance. Several researchers have studied the effect of cyclic loadings on RC beam-column connections strengthened with CFRP, experimentally for example; Gergely *et al.*, (1998) investigated the use of FRP for retrofitting piers of overpasses. Nine 1/3-scale T-shaped specimens were made and tested. Several casing configurations using advanced compound materials were applied to enhance the shear capability of the joints. Partial enhancements in the overall features of the specimens (such as peak load, ductility and energy-dissipation capacity) were witnessed. Although not explicitly addressed, the cause of the incomplete success is the problem related to confinement of rectangular sections. Pantelides *et*

Quick Response Code



Journal homepage:

<http://www.easpublisher.com/easjecs/>

Article History

Received: 04.02.2019

Accepted: 15.02.2019

Published: 25.02.2019

Copyright © 2019 The Author(s): This is an open-access article distributed under the terms of the Creative Commons Attribution 4.0 International License (CC BY-NC 4.0) which permits unrestricted use, distribution, and reproduction in any medium for non-commercial use provided the original author and source are credited.

DOI: 10.36349/easjecs.2019.v02i02.002

al., (1999) applied quasi-static lateral load tests of two full-scale RC bridge bents strengthened with carbon sheets in the cap beam-column joints; they concluded that the composite wrap increased the shear capacity of the joints. Gergely *et al.*, (2000) conducted some experimental studies on the subject of strengthening RC joints with FRP Laminates. They pointed out the increase in the strength of joints as a result of FRP strengthening of RC connections. Antonopoulos and Triantafillou (2003) conducted a comprehensive experimental program through two-thirds-scale testing of 18 exterior joints. Their study demonstrated the role of various parameters, e.g., area fraction of FRP and distribution of FRP, on shear strength of exterior joints. They also highlighted the importance of mechanical anchorages in limiting premature debonding. Ghobarah and El-Amoury (2005) have developed effective rehabilitation systems to upgrade the resistance to bond-slip of the bottom steel bars anchored in the joint zone and to upgrade the shear resistance of beam-column joints. Mukherjee and Joshi (2005) presented results of tests carried out on 13 interior beam-column joints. The parameters studied were: inadequate anchorage, FRP ratio; the type of FRP fibres and FRP retrofit scheme. All the retrofitted specimens failed by flexural hinging at the beam-joint interface. The test results clearly showed the effectiveness of the FRP system regardless of FRP schemes. Combined use of epoxy resin injection and FRP jacketing to rehabilitate RC beam-column joints was investigated by Karayannis and Sirkelis (2008). Their experiments showed that the use of epoxy resin can even restore the strength of a large-scale damaged joint and that application of FRP sheets can provide substantial further improvements on both load-carrying capacity and ductility. They also noted that failure in the retrofitted joints occurred outside the retrofitted area. Raman *et al.*, (2017) explored the plastic behavior of exterior beam-column joint under cyclic loading with different fiber reinforced concrete (FRC). The conclusion was that the use of fiber improves the damage tolerance behavior and ductility enhancement without sudden loss in strength.

There were some reports for the numerical analysis, a perfect bond was supposed between FRP sheets and concrete although experimental investigations showed that the debonding of CFRP sheets from concrete substrate is common mode of failure. For example using 3D analysis, Mahini and Ronagh (2011) observed the relocation of plastic hinges in beams, away from the beam-column joint using CFRP systems as a means of repair. It was concluded that beam hinges could be relocated further away from the joint by means of strengthening the joint with CFRP materials in the longitudinal direction. In another research, (Dalalbashi, A. *et al.*, 2012; Dalalbashi, A. *et al.*, 2013) showed that movement of the hinges can help increase the load carrying capacity of the structures. Failure in the beam leads to a localized failure and this is less devastating than a global failure ensuring from

the failure of the joints/column. Alhaddad *et al.*, (2011) attempted to predict their experimental results under cyclic loadings using the nonlinear FE models developed in ANSYS. A comparison of their numerical and experimental results indicated that their nonlinear FE models can accurately predict the experimental load-displacement curves up to the yielding point of longitudinal reinforcement. (Amit, Jindal. 2012) employed nonlinear FE analysis in ANSYS for modelling of a RC exterior beam-column joint retrofitted with externally bonded FRP. Using 2D analysis, (Sagbas *et al.*, 2011; H. Baji *et al.*, 2015) analysed beam-column joint subassemblies subjected to cyclic and monotonic loading in VecTor2 program and proposed general guidelines for effective FE modelling of RC beam-column joints. Using one dimensional analysis, (Eslami *et al.*, 2016) used FRP to confine columns at the critical zones of an 8-storey poorly-confined frame. Their results showed that the seismic performance and ductility increased substantially.

The primary purpose of the current investigation is to study experimentally various types of failure modes of RC exterior beam-column joints strengthened using CFRP sheets and develop a FE model able to predict all this failure modes to preclude brittle debonding failure, and shift the failure towards a beam.

Test program

Control specimen

A total of eight 2/3-scale beam-column T-joints were prepared and cast in the current study. The first specimen, C0, was considered as the base control specimen as shown in Fig. 1. It had an extruded beam of 900 mm length with 600 mm clear length from the loaded point to the face of the column. It had a cross-sectional dimensions of 200 × 400 mm. This beam was connected to a column at its mid-height point. The cross-section of the column was 200 × 200 mm. The total length of the columns was 2700 mm divided into two equal parts, lower part and upper part. The clear distance between lateral supports was 2300 mm. The upper and lower reinforcement of the beam in addition to the main longitudinal steel reinforcement of the column were made from high tensile steel. The top and bottom longitudinal reinforcement of the beam were three bars of 12 mm diameter each. On the other hand, the column was reinforced with one bar of 12 mm diameter at each corner of the column cross-section. The stirrups for both beam and column were mild steel bars of 8 mm diameter and spaced every 200 mm for the beam and the column, respectively. The clear concrete cover was taken as 15 mm. The test joints were designed such that the beam and columns have the same width and the beam was more heavily reinforced and more depth than the columns, resulting in strong beam / weak column design. In addition, three stirrups only were added at the beam-column joint. The test joints represent the common conditions and details of

old RC connections designed based on obsolete standards. By using the first principles of failure analysis, it is expected that the sequence of the failure for the control beam-column joint is joint shear failure followed by column hinging and finally followed by beam failure.

The concrete used in constructing the specimens was of 30MPa compressive strength, with maximum aggregate size of 20 mm and slump between 75 and 80 mm. The specimens were covered with burlap and cured for one week before removing the forms; they were then stored inside the laboratory until testing. At the start of the testing program, the specimens were approximately 2-months old. Testing was conducted over a 2-month period. Cylinders were tested in compression at 7 and 28 days. In addition, three cylinders were crushed on the day when each of the beam-column joints was tested. Nominal yield stress of reinforcement was 420 and 280 MPa for main steel and stirrups, respectively.

Strengthened specimens

Four different strengthening schemes were used as summarized in Table 2 and Fig. 2. The dimensions of CFRP sheets were designed according to first principles and were selected with relatively short

length to clearly manifest the debonding phenomena. One system consists of bonding the RC joint area and extended to specific lengths to the sides of the beams with one bi-direct layer of CFRP sheets (Specimen S1). Scheme S2 was similar to scheme S1 but the CFRP sheets extended to the back of the column in the form of a “U”. In schemes S1 and S2, the height of the CFRP bonding was limited to the depth of the beam at the joint. The CFRP sheets extend onto the beam to improve flexural and shear strength enhancement, which may adversely modify the relative strength ratios of the connected beam and column. Scheme S3 was identical to S1 but CFRP sheets applied in T shape where columns and beams were not wrapped. Scheme S4 was identical to S3 where beams and columns were wrapped to specific lengths. This system may be applied to strengthen the joint area as well as the column. The proposed strengthening schemes were expected to provide lateral confinement and shear resistance to the joint area, hence adding strength and ductility to the joint. By strengthening the shear resistance of the joint, the possibility of shear failure may be eliminated or delayed, which will create the opportunity to another mode of failure occurs such as hinging beam or column, rupture or debonding of CFRP.

The CFRP used was bi-directional carbon fibre, Table-1 shows the mechanical properties for both CFRP sheets along with the epoxy resins as provided by the manufacturer.

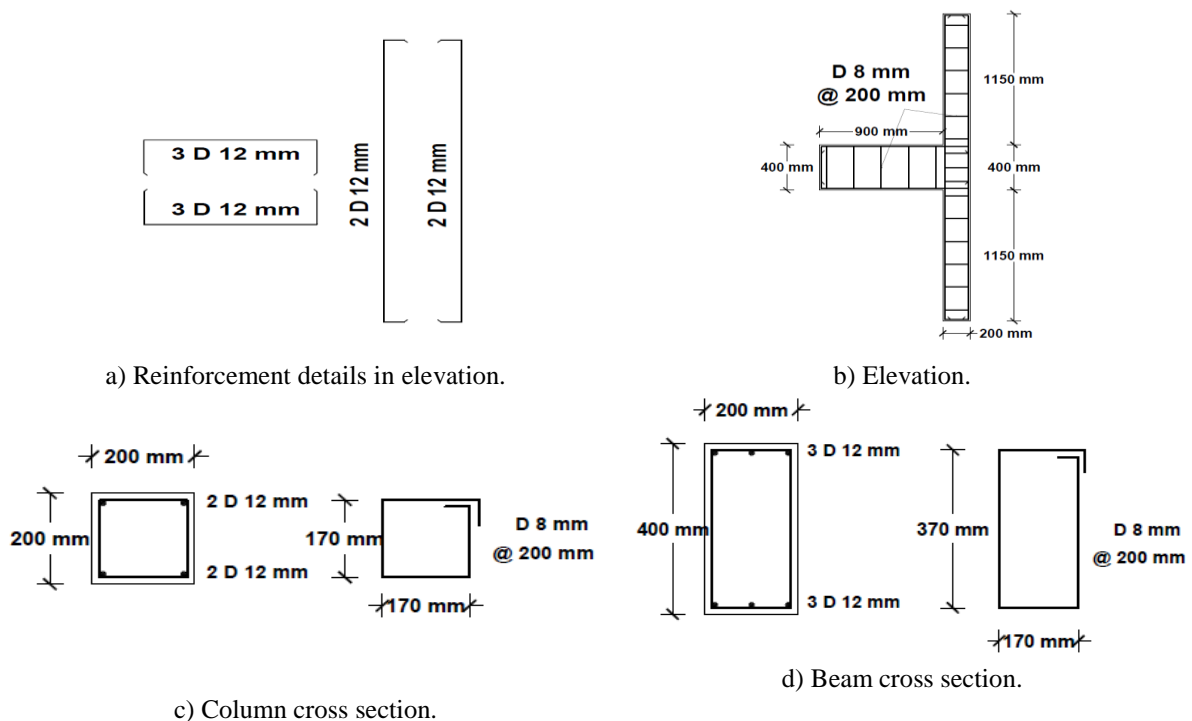


Fig.-1. The geometric and steel reinforcement of the RC beam-column connections.

Table-1. Mechanical properties of CFRP and epoxy.

Criteria	CFRP sheets	Epoxy
Tensile strength (MPa)	3500	30
Modulus of elasticity (GPa)	230	21.40
Failure strain (%)	1.50	4.80
Shear strength (MPa)	–	15.0
Thickness (mm)	0.165	–

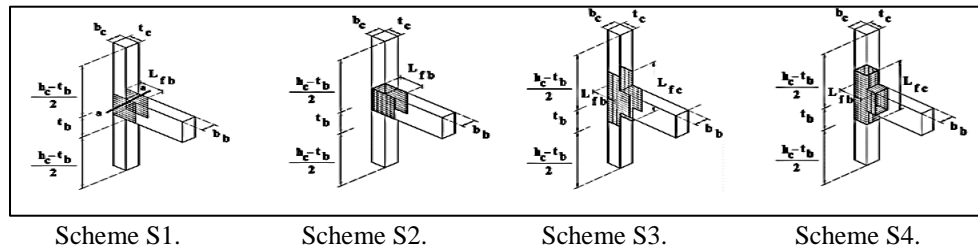


Fig. -2. CFRP layout for strengthened units.

To show the effect of the CFRP sheet length on the behavior of CFRP-strengthened RC beam-column connections, two RC beam-column connections from schemes S1, S3 and S4 with different lengths of CFRP sheets were used. Just one RC beam-column connection from scheme S2 was used.

Table- 2. Test specimens.

Strengthening scheme	Specimen designation	L_{fb}^* (mm)	L_{fc}^* (mm)
	C0	----	----
S1	S1-250	250	400
	S1-350	350	400
S2	S2-425	425	400
S3	S3-700	500	700
	S3-1000	500	1000
S4	S4-550	350	550
	S4-1000	350	1000

* L_{fb} and L_{fc} are defined in Fig. 2.

Experimental setup

The beam-tip displacement and the column lateral displacement were measured using potentiometers. Eight strain gauges were installed on the reinforcement steel bars to measure the strains at different loading levels, as shown in Fig. 3.

The strain gauges were named according to their positions:

- Strain gauges S1, S2 measures the normal strain developed on middle and top stirrups of the joint.
-

- Strain gauges S4, S6 and S8 measures the normal strain developed on the first stirrup located just ending of joint region (for control specimen) or CFRP region (for strengthened specimens) on the beam , upper and lower column respectively.
- Strain gauges S3, S5 and S7 measures the normal strain developed on the flexural reinforcement located just ending of joint region (for control specimen) or CFRP region (for strengthened specimens) on the beam , upper and lower column respectively.

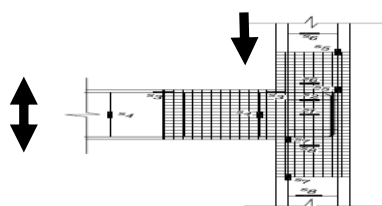


Fig.-3. Location of strain gauges on the reinforcement steel bars.

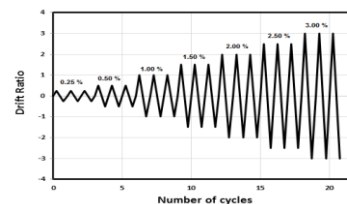


Fig.-4. Simulation of cyclic loading history.

The specimens were tested in the column vertical position, hinged at the top and bottom column ends with constant axial load applied to the column and subjected to a cyclic load applied at the beam tip as shown in Fig. 5. A constant axial load of 240 kN was applied to the column, using hydraulic jack provided with a load cell to measure the applied load. This load represents the gravity load that acts on the column, and was approximately equal to $0.2A_g \times f_c$, where A_g is the gross cross-sectional area and f_c is the compressive strength of concrete. The cyclic load was applied slowly to eliminate any dynamic effects. Typically, the loading of the specimen to failure required 30 to 45 minute to

complete. The cyclic load was applied at the beam tip using a hydraulic actuator of ± 250 mm stroke and was measured using a load cell. The loading was applied on the beam-column specimen according to the cyclic loading history shown in Fig. 4 according to Shwan and Hashim (2016), starting with a small drift ratio of 0.25% (The drift ratio is the ratio of the vertical beam tip displacement to the length from the centerline of the beam actuator to the centerline of the column). The drift continued with drift ratios of (0.5%, 1%, 1.5%, 2%, 2.5%, 3%... 6%). At each value of drift ratio, the cyclic loading was repeated three times.

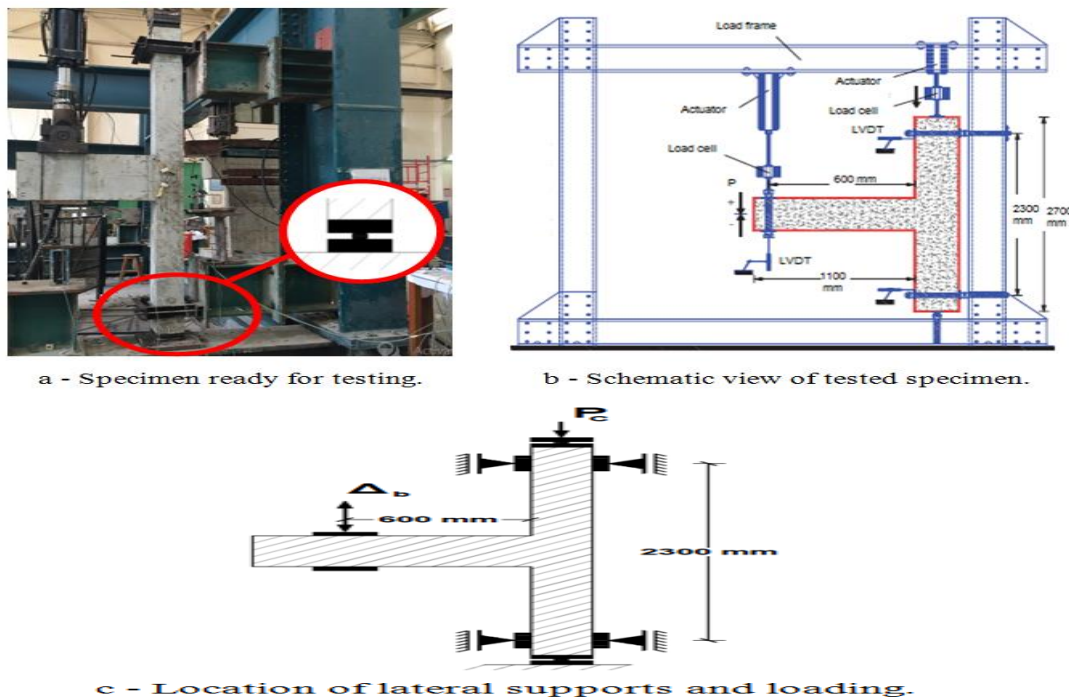


Fig.-5. Test setup for exterior beam-column joints.

TEST RESULTS AND DISCUSSION

Test results of control specimen

For the base control specimen C0: cracks began to appear at the upper end of the lower column under the joint region at a cyclic lateral load of about 15 kN. Increasing the cyclic lateral load led to increasing the propagation of cracks on the columns up to a cyclic lateral load of about 26 kN which cracks began to appear at the beam then diagonal shear crack was noted in the joint area in each loading direction, forming an X-pattern. At failure, these cracks extended to the back of the column as shown in Fig. 6-b. Considerable degradation in strength occurred at a drift ratio of 2 % (corresponding to beam-tip displacement of approximately 14 mm), which necessitated the termination of the test at a drift ratio of 3% (21 mm), as the load sustained by the specimen had dropped to 48% of the maximum load.

Test results of strengthened specimens

The results from the testing of joints S1-250 and S1-350 are very similar to the control specimen C0. During the test, the CFRP delaminated as the joint shear cracking occurred under the CFRP sheet. The cracking progressed until the joint failed. The specimen S1-250 was suffered from debonding of CFRP sheet by concrete cover separation mode which started to debond from the beam face and the ultimate capacity increased by 15% (see Fig. 6-c, 6-d). In contrast, the specimen, S1-350 was suffered from debonding of CFRP sheet (by concrete cover separation mode) which started to debond from the direction of the back of the column and the ultimate capacity increased by 21% (see Fig. 6-e, 6-f). Tests results of joints S1-250 and S1-350 indicate that: the debonding direction of CFRP varies depending on the CFRP sheet length and using web bonded CFRP scheme did not contribute much to the shear strengthening of the joint because the debonding

takes place which is considered as unacceptable strengthening scheme.

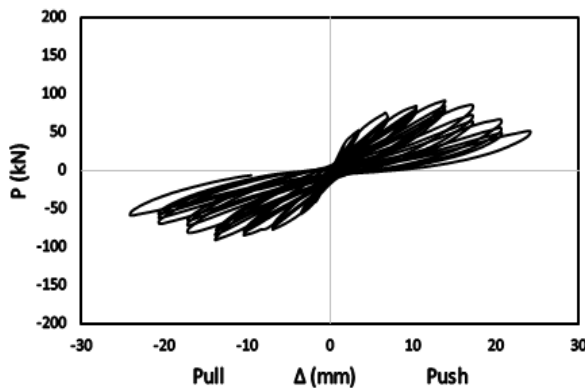
Joint specimen S2-425 performed well. The joint sustained a maximum beam-tip load of 103.3 kN (ultimate capacity increased by 29%). Throughout the test, no CFRP debonding was observed and no shear cracking developed in the joint area. Instead, the failure was due to ductile plastic flexural hinging in the columns. This strengthening scheme was successful in preventing the beam-column joint shear failure however, it is considered unacceptable strengthening scheme causing column hinging mode failure. The final failure mode of the joint is shown in Fig. 6-h.

For specimens S3-700 and S3-1000, partial debonding was observed at a drift ratio of 2% (14 mm) and near the middle of the CFRP region from the column edge (see Fig. 6-j, 6-l), as slight fingertip tapping on the CFRP revealed a hollow sound. The debonded area was increased until all the CFRP separated from the column sides. During the test, the CFRP delaminated as the joint shear cracking was occurred under the CFRP zone. The cracking progressed until the joint failed in shear with a similar manner to the control specimen C0. The ultimate capacity increased by 28% and 30% for S3-700 and S3-1000 respectively. Tests results of joints S3-700 and S3-1000 indicate that: increasing the bonded area of CFRP using S3 scheme (CFRP sheets applied in T shape where columns and beams were not wrapped.) did not contribute much to the shear strengthening of

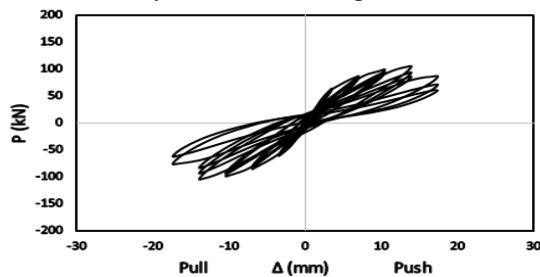
the joint because the debonding takes place which is considered as unacceptable strengthening scheme.

In specimen S4-550, initial cracking was observed in the upper end of the lower column under the joint region, pointing to flexural hinge formation. The CFRP layers used were successful in delaying both the joint shear failure and debonding failure while a ductile flexural plastic hinge was forming in the columns. The failure pattern of specimen S4-550 is shown in Fig. 6-n. The ultimate capacity increased by 37%.

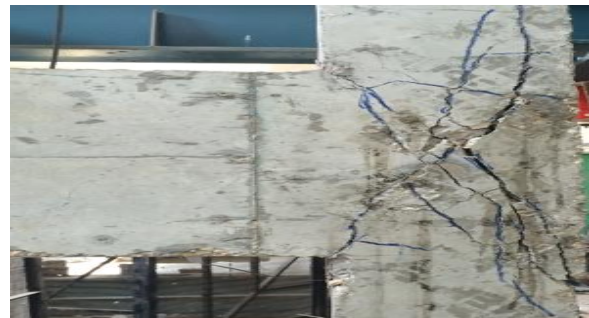
In specimen S4-1000, the first crack was recorded at upper end of the lower column under the joint region. However, a shear hinge in the beam, of length approximately equal to the depth of the beam, developed starting from the face near the end of the CFRP sheet from the beam direction. The strengthening scheme used here was successful in delaying the joint shear failure, debonding failure and column hinging failure; however, shear failure of the beam occurred. This is attributed to the limited number of stirrups in the beam. This means that even when the CFRP strengthening scheme could eliminate the joint shear failure, some attention should be paid to increase the shear capacity of the beam to ensure ductile moment failure mode. The failure pattern of specimen S4-1000 is shown in Fig. 6-p. The ultimate capacity increased by 65%. Table 3 summarizes the recorded failure characteristics after complete collapse of all specimens.



a- The hysteretic curve of specimen C0.



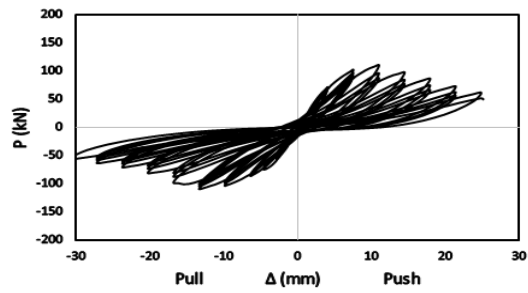
c- The hysteretic curve of specimen S1-250.



b- Failure condition of specimen C0.



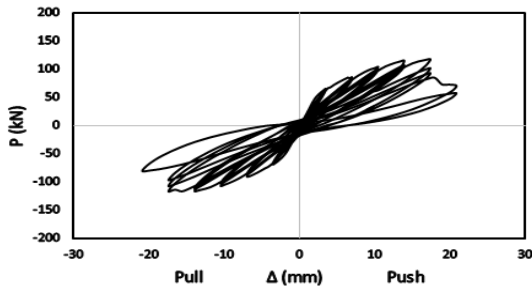
d- Failure condition of specimen S1-250.



e- The hysteretic curve of specimen S1-350.



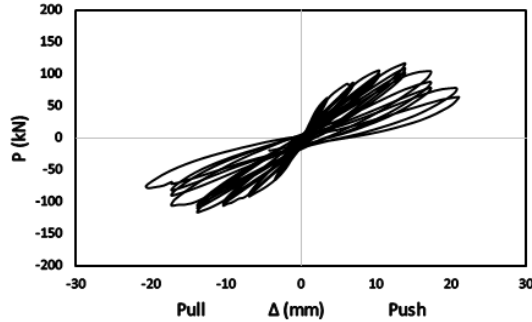
f- Failure condition of specimen S1-350.



g- The hysteretic curve of specimen S2-425.



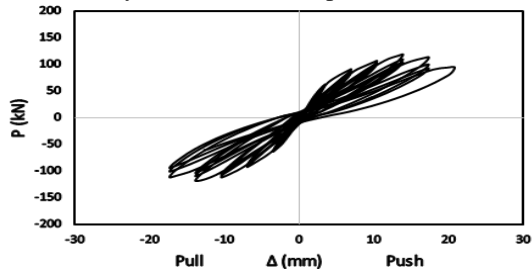
h- Failure condition of specimen S2-425.



i- The hysteretic curve of specimen S3-700.



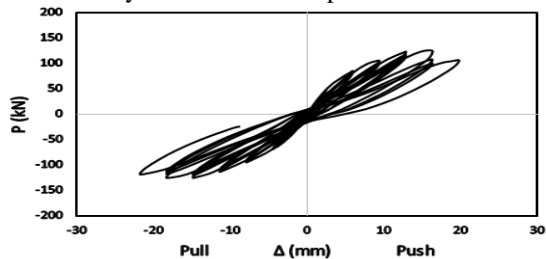
j- Failure condition of specimen S3-700.



k- The hysteretic curve of specimen S3-1000.



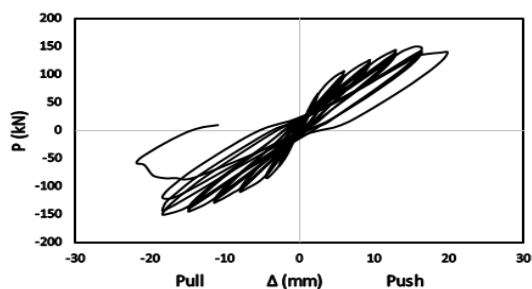
l- Failure condition of specimen S3-1000.



m- The hysteretic curve of specimen S4-550.



n- Failure condition of specimen S4-550.



o- The hysteretic curve of specimen S4-1000.

p- Failure condition of specimen S4-1000.

Fig.-6. The hysteretic curves and Failure conditions for all beam-column joints.

DISCUSSION

In this section, the hysteretic behavior, stiffness degradation and energy dissipation of the tested specimens are discussed.

The envelopes of the hysteretic loops of the tested specimens are shown in Fig. 7. Specimen S4-1000 showed almost 65% increase in the load-carrying capacity compared with control specimen C0. The pinching effect is severe in specimen C0 as compared with specimen S4-1000 (see Fig. 6-a, Fig. 6-o).

Table- 3. Experimental results and failure characteristics of all specimens after complete collapse.

Specimen	Cracking load (kN)		Ultimate load (kN)	Deflection at ultimate load (mm)	Ultimate strain at failure, micro-strain								Dominant mode of failure
	Beam	Column			S1	S2	S4	S6	S8	S3	S5	S7	
C0	17.80	10.70	90.90	13.17	1500	1450	153	161	244	1900	1836	1800	Shear failure at the joint
S1-250	19.40	10.70	105.00	13.66	1690	1500	62.5	335	189	1747	1600	1700	De-bonding of CFRP sheet followed by shear failure at the joint
S1-350	23.70	10.70	110.00	10.78	1700	1520	28	290	230	1400	1900	1800	
S2-425	28.40	10.70	117.50	17.4	687	685	130	320	246	1080	25000	25600	Flexural failure of the column
S3-700	35.50	12.70	116.60	13.27	1700	1680	10	135	100	685	1810	1410	De-bonding of CFRP sheet followed by shear failure at the joint
S3-1000	35.50	15.60	118.40	13.34	1780	1700	12	88	66	904	1760	1180	
S4-550	23.70	11.60	125.00	16.50	858	731	121	214	147	1870	13690	2900	Flexural failure of the columns
S4-1000	23.70	15.60	150.00	17.00	537	565	1590	123	55	1900	1800	1350	Shear failure of the beam

The bold value means that strain exceeded the yield strain.

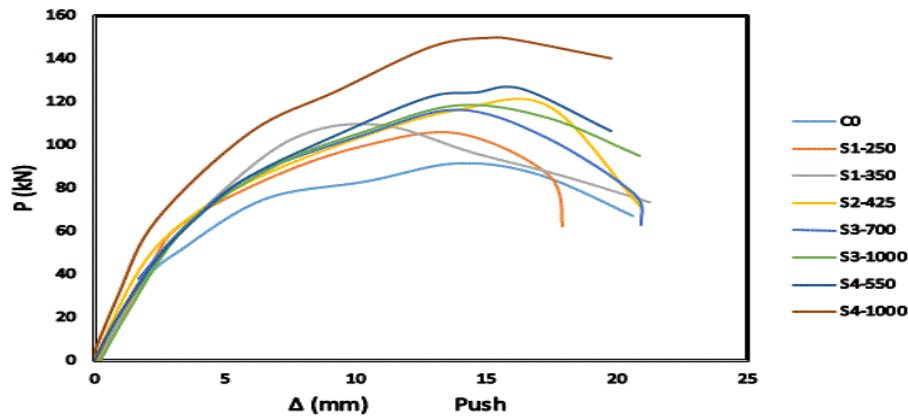


Fig.-7. Hysteretic loop envelopes of the test specimens.

The beam-column joint stiffness was approximated as the slope of the peak-to-peak line in each loop. Test results indicated that stiffness degradation (as shown in Fig. 8) was due to various factors such as non-linear deformations, flexural and shear cracking, distortion of the joint panel, slippage of reinforcement, and loss of cover and debonding of

CFRP sheets. As shown in Fig. 8, strengthened specimens exhibit larger stiffness at the initial stage of loading. Due to premature failure of CFRP by debonding or shear failure of the beam, stiffness of specimens S3-700, S3-1000 and S4-1000 decreases rapidly as compared with other strengthened specimens.

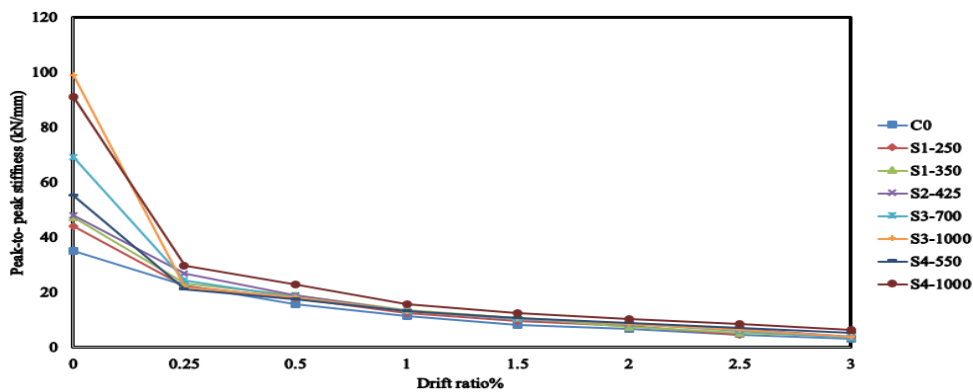


Fig.-8. Degradation of stiffness with beam drift.

The area enclosed by a hysteretic loop at a given cycle represents the energy dissipated by the specimen during this cycle. The capability of a structure to dissipate energy has a strong influence on its

response to an earthquake loading. Fig. 9 shows the cumulative energy dissipated by the eight beam-column joints. Specimen S4-1000 is able to dissipate more energy compared with control specimen C0.

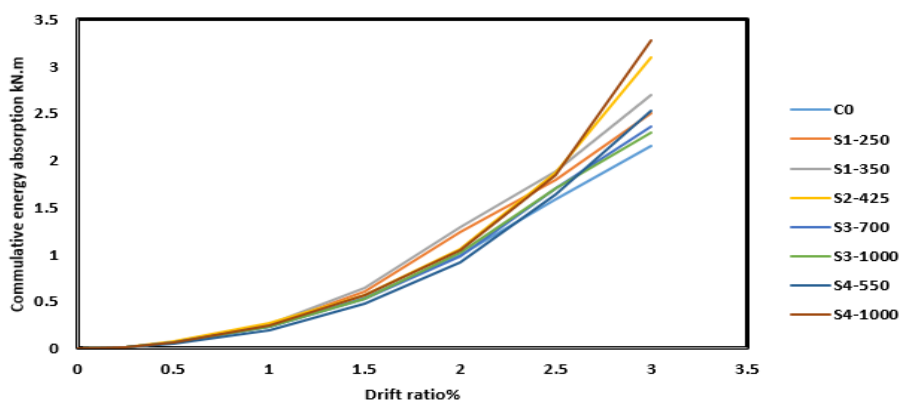


Fig.-9. Cumulative energy dissipated by the tested specimens.

Finite Element Analysis

In order to obtain an efficient and accurate finite element method, the analysis was conducted in ABAQUS/Standard module (Karlsson, H., & Sorensen.2000). All parts of models are presented detailedly as follows.

Modeling in 2D space gives the same results of 3D with high accuracy and less required time and computational capacity so the beam-column connections and CFRP are modeled based on quadrilateral plane stress elements (SPS4R), Mesh elements consist of a four node. All elements with reduced integration function, the reinforcements have been modeled with a 2-node linear truss element

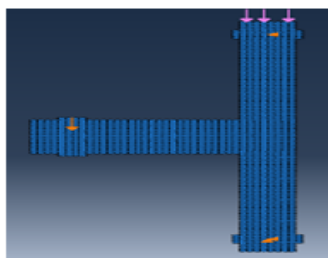


Fig.-10. Geometry and elements used in the numerical analysis.

To represent the two failure modes, concrete cover separation or sheet debonding, three layers of 2D shell elements were used, the first layer represents the concrete core thickness, the second layer represents twice of the concrete cover thickness and the third layer represents twice of the CFRP thickness. Two sets of connectors were used, the first set used to connect the first and the second layer and represents the concrete behavior in shear to capture concrete cover separation mode failure (C.C.S) while the second set used to connect the second and third layer and represents the epoxy behavior in shear to capture sheet debonding mode failure (debonding).

The bond between concrete and CFRP sheets was modelled using a cohesive surface model. Fig. 11 shows a graphic interpretation of a simple bilinear traction–separation law written in terms of the effective traction τ and effective opening displacement δ . The interface is modelled as a rich zone of small thickness.

From Fig. 11, it is obvious that the relationship between the traction stress and effective opening displacement is defined by the stiffness, K_0 , the local strength of the material, τ_{max} , a characteristic opening displacement at fracture, δ_f , and the energy needed for opening the crack, G_{cr} , which is equal to the area under the traction– displacement curve. Lu XZ *et al.*, (2005) provides an upper limit for the maximum shear stress, τ_{max} , giving $\tau_{max} = 3$ MPa in the case of using a high

(T2D2). Fig. 10 shows Geometry and elements used in the numerical analysis.

In ABAQUS reinforcement can be modeled with different methods including smeared reinforcement in the concrete, cohesive element method, discrete truss or beam elements with the embedded region constraint or built-in rebar layers. In this part, just embedded region (perfect bond) modeling used for reinforcement .According to Karlsson, H., & Sorensen. (2000) the effect of bond slip is not considered in the embedded region modeling method but this effect is considered somewhat by definition of the tension stiffening behavior of concrete.

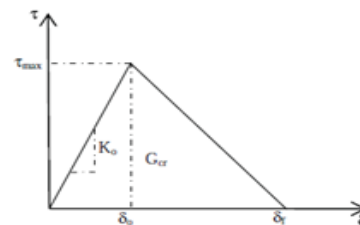


Fig.-11. Bilinear traction–separation constitutive law.

strength epoxy. Previous researches, Obaidat *et al.*, (2010) studied numerically and showed that this value is too high; since CFRP rupture or concrete crushing induced the failure, instead of the CFRP debonding that occurred in the experimental studies in the literature. Previous researches (JCI 1998; JCI.2003) studied numerically the fracture energy, G_{cr} . The initiation of damage was assumed to occur when a quadratic traction function involving the nominal stress ratios reached the value one. Interface damage evolution was expressed in terms of energy release. The description of this model is available in (Karlsson, H., & Sorensen. 2000). The dependence of the fracture energy on the mode mix was defined based on the Benzaggah–Kenane fracture criterion. Benzaggah–Kenane fracture criterion is particularly useful when the critical fracture energies during deformation purely along the first and the second shear directions are the same.

In this study the parameters of cohesive surface represent the interface between CFRP and concrete were taken according to Obaidat *et al.*, (2010). There are 1.5 MPa, 508 N/mm³ and 900 J/m² for τ_{max} , K_0 and G_{cr} respectively.

The mechanical properties of concrete were modeled using ABAQUS’s own Concrete Damage Plasticity (CDP) formulation. The concrete compression hardening curve was fitted to the stress–strain relationship of the cylinder compression test while the

concrete tension curve was fitted to the stress–displacement relationship. The degradation of the elastic stiffness in tension and compression was inserted using The CONCRETE DAMAGE parameters.

The compressive strength f_c in the experimental work was measured to be 30 MPa. $E_c = 26$ GPa. The stress–strain relationship proposed by Saenz (1964) was used to construct the uni-axial compressive stress–strain curve for concrete, Poisson’s ratio for concrete was assumed to be 0.2 and f_{ct} (The tensile strength of concrete) was then calculated by

$$f_{ct} = 0.33\sqrt{f_c} \approx 1.8 \text{ MPa.} \tag{1}$$

To specify the post-peak tension failure behavior of concrete the fracture energy method was used. The fracture energy for mode I, G_f , is the area under the softening curve. The stiffness degradation damage proposed by Jankowiak, lodygowski (Jankowiak, T., & Lodygowski, T. 2005) was used.

When steel members suffer from cyclic loadings, a steel constitutive model of cyclic plasticity is needed, which is different from the monotonic model. The constitutive model of structure steel under cyclic loading plays a quite important role in structural seismic design and analysis. Currently, steel stress–strain relationship is commonly defined as bilinear or multi-linear forms. Those models, however, cannot satisfy cyclic loading conditions as studied by SHI YJ (2011). From Shi, G. *et al.*, study (2012), a conclusion that the results calculated from cyclic model of steel were in a better agreement with experiments for both loading and reloading processes could be obtained. The cyclic model well predicted the structural hysteretic behaviors by SHI YJ (. In terms of the cyclic tests of steel in Shi G study (2012), the cyclic hardening criterion of steel is

a combining one, containing both isotropic hardening and kinematic hardening. (Chaboche, J. L.1986; Chaboche, J.L. 1989) proposed a cyclic combined model based on plastoelasticity. This model was implemented in ABAQUS as a plastic constitutive model of metal, consisting of a nonlinear kinematic hardening component and an isotropic hardening component.

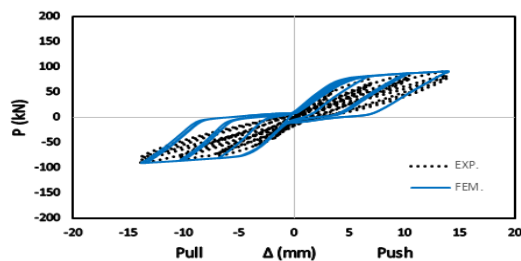
The parameters of cyclic hardening according to the help files of ABAQUS are σ_{10} , Q_∞ , b_{iso} , C_{kin} , γ . where σ_{10} is the yielding stress at zero plastic strain, Q_∞ is the maximum change in the size of yielding surface, b_{iso} is the rate at which the size of yielding surface changes as plastic straining develops, C_{kin} is the initial kinematic hardening moduli and γ is the rate at which the kinematic hardening moduli decrease with the increasing plastic deformation.

Parameters of cyclic hardening for flexural steel used in ABAQUS are 420 N/mm², 13000.0 N/mm², 44.06, -200 N/mm², 80.0 for σ_{10} , C_{kin} , γ , Q_∞ and b_{iso} respectively.

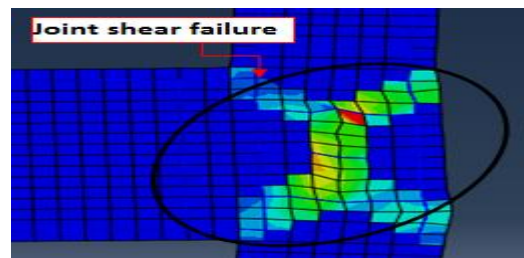
The CFRP material was considered as linear elastic isotropic until failure. A Poisson’s ratio of 0.3 was used for the CFRP material. The elastic modulus E_f , and the ultimate stress f_{pu} are the values needed to draw the stress strain curve for the CFRP material.

Experimental–Numerical Comparison and Improvements

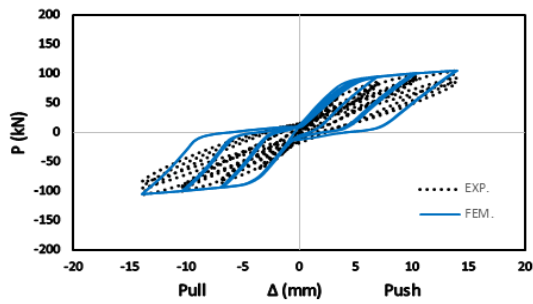
The numerical simulations agree well with test results as shown in Fig. 12 including hysteretic curves and failure modes, indicating that the numerical method could accurately predict the behaviors of RC beam-column connections strengthened with CFRP. In addition, from the compared hysteretic curves, the model can simulate the degradation of strength and stiffness as well as the pinching effect.



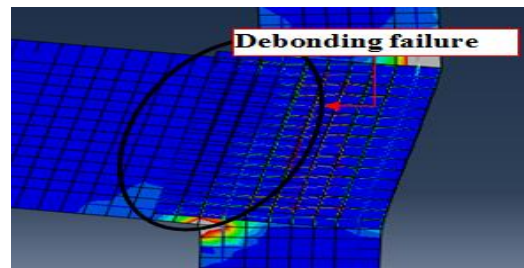
- The hysteretic curves for specimen C0.



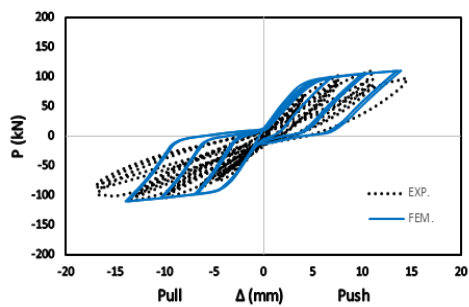
b- Plastic strain distribution for specimen C0.



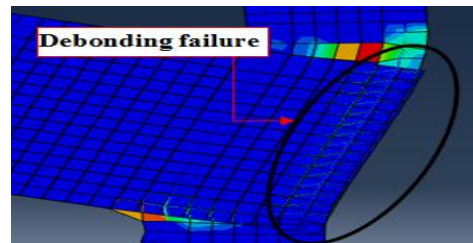
c- The hysteretic curves for specimen S1-250.



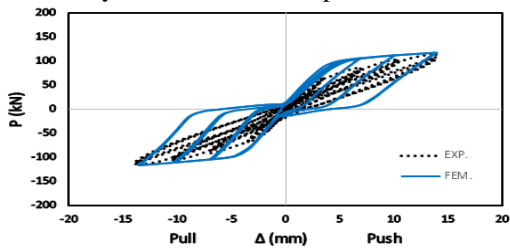
d- Plastic strain distribution for specimen S1-250.



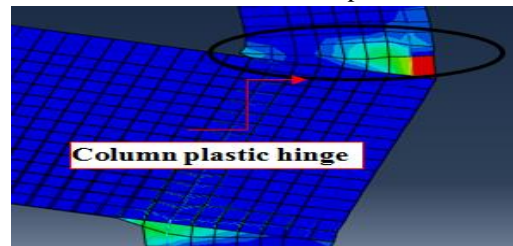
e- The hysteretic curves for specimen S1-350.



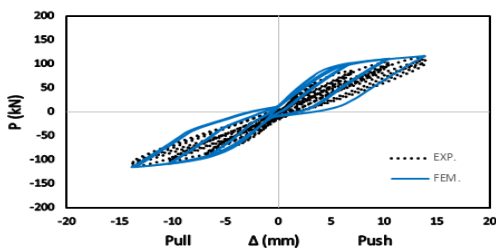
f- Plastic strain distribution for specimen S1-350.



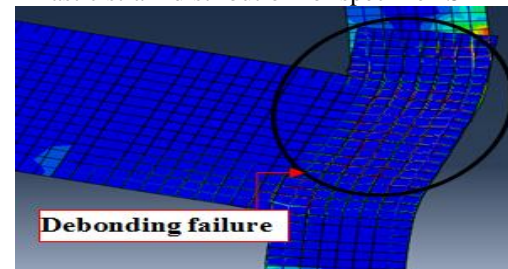
g- The hysteretic curves for specimen S2-425.



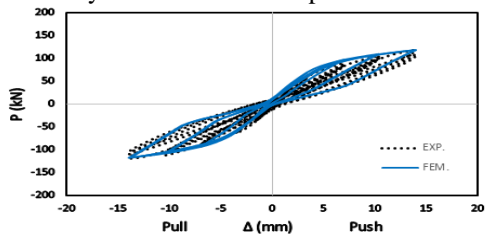
h- Plastic strain distribution for specimen S2-425.



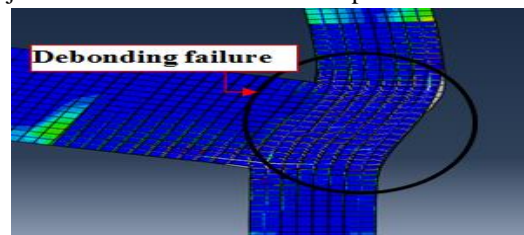
i- The hysteretic curves for specimen S3-700.



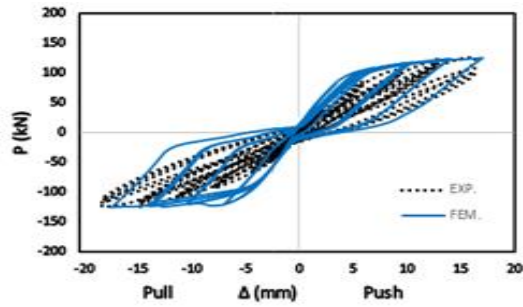
j- Plastic strain distribution for specimen S3-700.



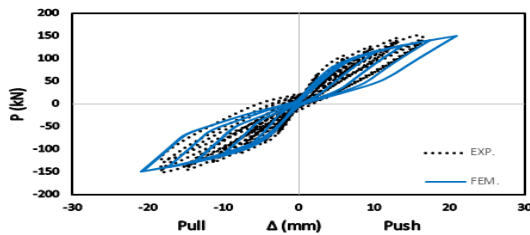
k- The hysteretic curves for specimen S3-1000.



l- Plastic strain distribution for specimen S3-1000.



m- The hysteretic curves for specimen S4-550.



o- The hysteretic curves for specimen S4-1000.

Fig.-12. The hysteretic curves and plastic strain distribution for all specimens.

As seen in Fig. 12-p specimen S4-1000 suffered from brittle shear failure of the beam. Shear failure as is known occurs very suddenly and in a brittle fashion. Therefore to avoid this shear failure which is considered as undesirable failure mode, the effect of adding additional external CFRP strips for beam of specimen S4-1000 was studied numerically to increase the shear capacity of the beam and preclude brittle beam shear failure to transfer the failure mode to a ductile beam plastic hinging. Also due to premature debonding of CFRP that noted in scheme S3 (See figures 12-j and 12-l), the effect of using steel anchors for scheme S3 was also studied numerically to delay the debonding.

Fig. 13 shows specimen (S4-1000-M), it is similar to specimen S4-1000 but with adding additional external CFRP strips that used to strengthen the beam in shear by wraps (50 mm wide × 0.165 mm thick), spaced every 100 mm and started 50 mm from the end of T wrap.

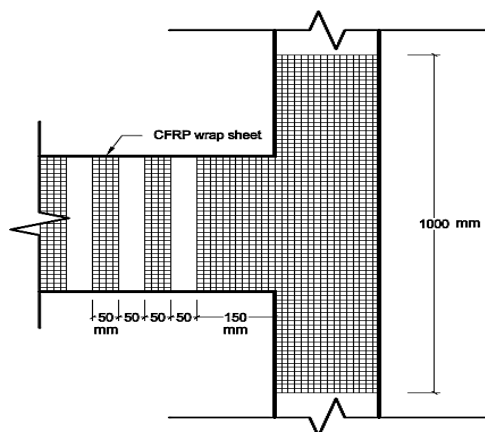
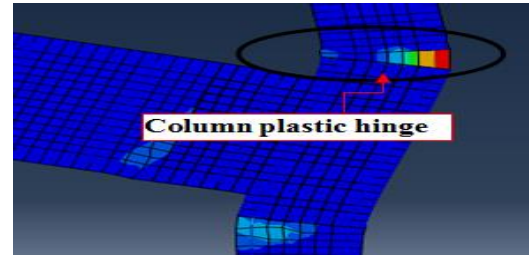
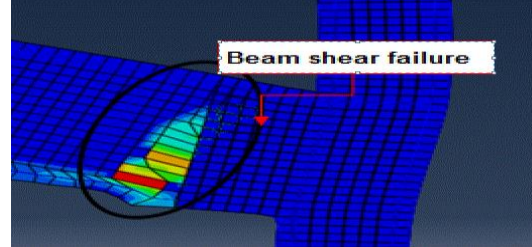


Fig.-13. Layout of specimen S4-1000-M.



n- Plastic strain distribution for specimen S4-550.



p- Plastic strain distribution for specimen S4-1000.

Fig. 14 shows specimen (S3-1000-M), it is similar to (S4-1000-M) but scheme S3 was used instead of S4. It provided with additional improvement by preventing the CFRP from debonding where scheme S3 was anchored using eight steel plates and twenty four steel anchors driven through the connection.

To represent the actual behavior of anchors, rigid plastic CARTESIAN elements from the ABAQUS library (Karlsson, H., & Sorensen.2000) were used. Connector behaviors can be defined in any connector with available components of relative motion. Available components of relative motion are displacements and rotations that are not kinematically constrained. Multiple connector behaviors can be defined in the connector section (Karlsson, H., & Sorensen.2000). To model a Cartesian connector that represents an anchor, taking into consideration shear deformations, 'Plasticity and elasticity' behaviors were defined in the anchor shear force directions.

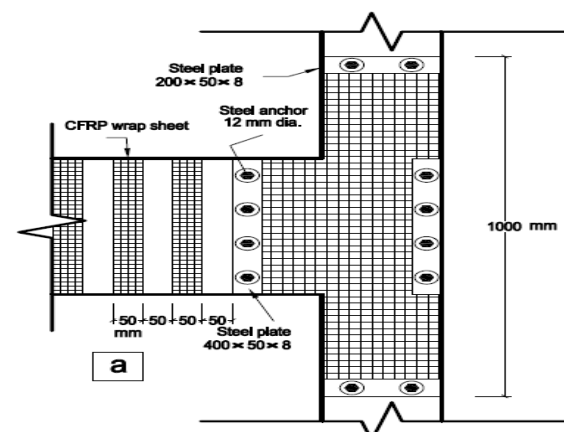


Fig.-14. Layout of specimen S3-1000-M.

Both analyzed specimens (S4-1000-M and S3-1000-M) showed a ductile behavior without any shear/shear-flexural cracking at the beam or the joint core, no debonding or delamination was observed during the analysis. The numerical results confirmed the weak-beam strong-column condition adopted in the recently design codes. During the cyclic loading, flexural cracks were developed and widened in the plastic hinge areas of the strengthened specimens, while the column remained intact.

The envelope of beam tip load–displacement curves obtained from the numerical analysis of the specimens under cyclic loads is compared in Fig. 15. Hinging pattern of the strengthened specimens, illustrate in Fig. 16, shows the capability of the adopted strengthening methods in relocating of the plastic hinge away from the beam-column interface. This type of failure with plastic hinges away from the column interface is desirable in seismic strengthening in order to prevent the joint brittle failure or column hinging.

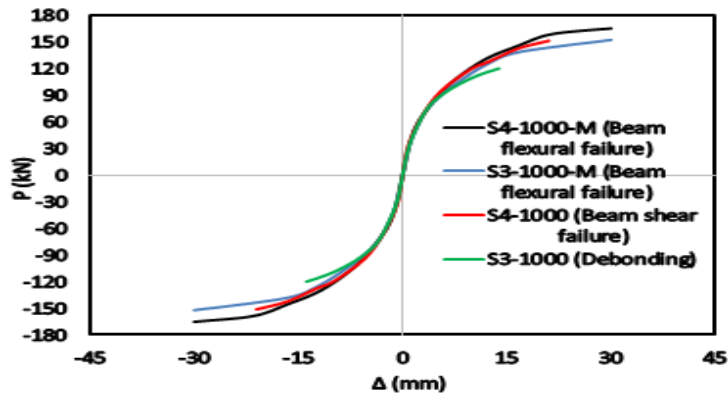


Fig.-15. Hysteretic loop envelopes of numerical analysis up to ultimate load.

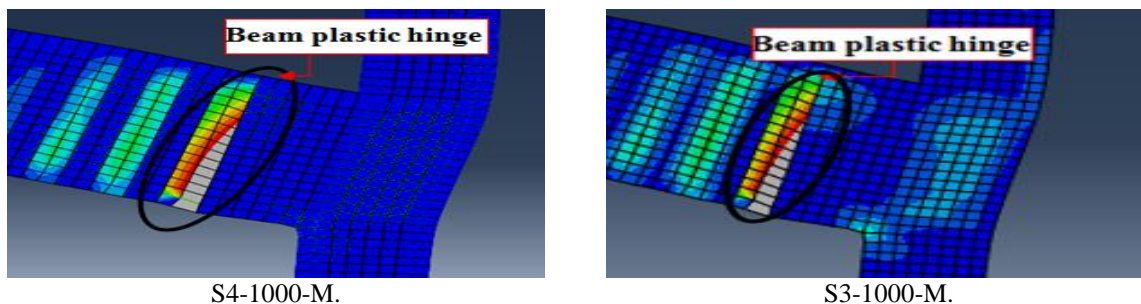


Fig.-16. Plastic strain distribution for strengthened specimens.

CONCLUSIONS

The paper investigated the behavior of RC beam-column connections strengthened with CFRP. The following conclusions are drawn from experimental tests and numerical simulations:

- When using web bonded CFRP scheme (without extended to the back of the column (scheme S1)), increasing the length of CFRP leads to relocate the debonded zone from the beam direction to the joint direction.
- Increasing the bonded area of CFRP sheets that applied in T shape where columns and beams were not wrapped did not contribute much to the strengthening of the joint or the column because the debonding takes place (as specimens S3-700 and S3-1000).
- CFRP strengthening scheme may change the mode of failure of RC beam-column connections from joint shear failure to unaccepted hinging column failure in the cases of the flexural capacity of the column cross section considering axial load is smaller than that of the beam.
- Employing externally bonded CFRP sheets that applied in T shape where beams and columns were fully wrapped to specific lengths resulted in an increase in maximum load reached values of about 65% (as specimen S4-1000).
- The proposed finite element model could give a quite accurate prediction for the behaviors of RC beam-column connections strengthened with CFRP under cyclic loading taking the effect of debonding between CFRP and concrete, including carrying capacity, hysteretic curves and varies probable

failure modes. It proved the rationality of selected element types, constitutive models and contact models comparing the experimental results. The finite element model provided a strong tool for studying the performance of RC beam-column connections strengthened with CFRP.

- Using two cohesive surfaces succeeded to capture the main two failure modes either concrete cover separation at the surface just outside the stirrups of the joint or sheet debonding at the surface below the adhesive. The cohesive model proved its ability to represent the bond behavior between the aforementioned surfaces.
- If there is a difficulty on applying full wrapping system, using steel anchors, if appropriately installed, can significantly increase both the capacity and the ductility of the RC beam-column connection strengthened with CFRP. The failure mode can be changed from CFRP debonding failure or concrete cover separation to beam plastic hinging failure.

REFERENCES

1. Gergely, I., Pantelides, C. P., & Reaveley, L. D. (1998). Shear strengthening of bridge joints with carbon fiber composites. In *Proceedings of Sixth US National Conference on Earthquake Engineering, Seattle, WA, USA* (Vol. 31).
2. Pantelides, C. P., Gergely, J., Reaveley, L. D., & Volnyy, V. A. (1999). Retrofit of RC bridge pier with CFRP advanced composites. *Journal of Structural Engineering*, 125(10), 1094-1099.
3. Gergely, J., Pantelides, C. P., & Reaveley, L. D. (2000). Shear strengthening of RCT-joints using CFRP composites. *Journal of composites for construction*, 4(2), 56-64.
4. Antonopoulos, C. P., & Triantafillou, T. C. (2003). Experimental investigation of FRP-strengthened RC beam-column joints. *Journal of composites for construction*, 7(1), 39-49.
5. Ghobarah, A., El-Amoury, T. (2005). Seismic rehabilitation of deficient exterior concrete frame joints. *ASCE*, 9(5):408-16.
6. Mukherjee, A., Joshi M. (2005). FRPC reinforced concrete beam-column joints under cyclic excitation. *Composite Structures*; (70),185-99.
7. Karayannis, C. G., & Sirkelis, G. M. (2008). Strengthening and rehabilitation of RC beam-column joints using carbon-FRP jacketing and epoxy resin injection. *Earthquake Engineering & Structural Dynamics*, 37(5), 769-790.
8. Bharti, R., Chidambaram, R. S., & Kwatra, N. (2017). Influence of Fiber Reinforced Concrete on Plastic Behavior on Exterior Beam Column Joint under Cyclic Loading. *Procedia engineering*, 173, 1122-1129.
9. Mahini, S. S., & Ronagh, H. R. (2011). Web-bonded FRPs for relocation of plastic hinges away from the column face in exterior RC joints. *Composite Structures*, 93(10), 2460-2472.
10. Dalalbashi, A., Eslami, A., & Ronagh, H. R. (2012). Plastic hinge relocation in RC joints as an alternative method of retrofitting using FRP. *Composite Structures*, 94(8), 2433-2439.
11. Dalalbashi, A., Eslami, A., & Ronagh, H. R. (2013). Numerical investigation on the hysteretic behavior of RC joints retrofitted with different CFRP configurations. *Journal of Composites for Construction*, 17(3), 371-382.
12. Alhaddad, M. S., Siddiqui, N. A., Abadel, A. A., Alsayed, S. H., & Al-Salloum, Y. A. (2011). Numerical investigations on the seismic behavior of FRP and TRM upgraded RC exterior beam-column joints. *Journal of Composites for Construction*, 16(3), 308-321.
13. Jindal, A. (2012). Finite element modelling of reinforced concrete exterior beam-column joint retrofitted with externally bonded fiber reinforced polymer (FRP) Master's Thesis, *Thapar University*
14. Sagbas, G., Vecchio, F., Christopoulos, C. (2011), Computational modeling of the seismic performance of beam-column subassemblies. *Journal of earthquake engineering*, (15), 640-63.
15. Baji, H., Eslami, A., & Ronagh, H. R. (2015, August). Development of a nonlinear FE modelling approach for FRP-strengthened RC beam-column connections. In *Structures*(Vol. 3, pp. 272-281). Elsevier.
16. Eslami, A., & Ronagh, H. R. (2013). Effect of FRP wrapping in seismic performance of RC buildings with and without special detailing—A case study. *Composites Part B: Engineering*, 45(1), 1265-1274.
17. Said, S. H., & Razak, H. A. (2016). Structural behavior of RC engineered cementitious composite (ECC) exterior beam-column joints under reversed cyclic loading. *Construction and Building Materials*, 107, 226-234.
18. Karlsson, H., & Sorensen. (2000). Inc. ABAQUS Theory manual, User manual and Example Manual, Version. Providence, 6-7.
19. Lu, X. Z., Teng, J. G., Ye, L. P., & Jiang, J. J. (2005). Bond-slip models for FRP sheets/plates bonded to concrete. *Engineering structures*, 27(6), 920-937.
20. Obaidat, Y. T., Heyden, S., & Dahlblom, O. (2010). The effect of CFRP and CFRP/concrete interface models when modelling retrofitted RC beams with FEM. *Composite Structures*, 92(6), 1391-1398.
21. JCI. (1998), Technical report on continuous fibre reinforced concrete. JCI TC952 on continuous reinforced concrete. p. 116-24.
22. JCI. (2003), Technical report on retrofit technology for concrete structures. Technical committee on retrofitting technology for concrete structures. p. 79-97.
23. Saenz, L. P. (1964). "Equation for the Stress-Strain Curve of Concrete." *ACI J* 61 (9), 1229-1235.

24. Jankowiak, T., & Lodygowski, T. (2005). Identification of parameters of concrete damage plasticity constitutive model. *Foundations of civil and environmental engineering*, 6(1), 53-69.
25. Shi, Yongjiu, Meng Wang, and Yuanqing Wang. "Experimental and Constitutive Model Study of Structural Steel under Cyclic Loading." *Journal of Constructional Steel Research* 67.8 (2011): 1185–1197.
26. Shi, G., Wang, M., Bai, Y., Wang, F., Shi, Y., & Wang, Y. (2012). Experimental and modeling study of high-strength structural steel under cyclic loading. *Engineering Structures*, 37, 1-13.
27. Chaboche, J. L. (1986). Time-independent constitutive theories for cyclic plasticity. *International Journal of plasticity*, 2(2), 149-188.
28. Chaboche, J.L. (1989) "Constitutive Equations for Cyclic Plasticity and Cyclic Viscoplasticity." *International journal of plasticity*, 5(3) 247–302.